https://doi.org/10.1016/j.apenergy.2021.118405

Revised Ms APEN-D-21-06895

(Original Research Article)

Cooling storage performance of a novel phase change material nano-emulsion for room air-conditioning in a self-designed pilot thermal storage unit

Liu LIU [a], Xiyao ZHANG [a, d], Haobin LIANG [b, c], Jianlei NIU [b] and Jian-Yong WU [a, *]

[a] Department of Applied Biology & Chemical Technology, The Hong Kong Polytechnic University, Hung Hom, Kowloon, Hong Kong

[b] Building Environment and Energy Engineering, The Hong Kong Polytechnic University, Hung Hom, Kowloon, Hong Kong

[c] School of Civil Engineering, The University of Sydney, NSW 2006, Sydney, Australia

[d] Xiyao ZHANG's current affiliation: Nano and Advanced Materials Institute Ltd., The Hong Kong University of Science and Technology, Hong Kong Science Park, New Territories, Hong Kong (e-mail: xiyaozhang@ust.hk)

* Corresponding author:

E-mail address: Jian-yong.wu@polyu.edu.hk (J.Y. Wu).

ABSTRACT

The dynamic stability of phase change material (PCM) emulsions is a crucial factor for their practical applications. So far most previous studies on PCM emulsions have been focused on the static stability in the laboratory and cooling performance in small scale systems, but not few or none on the dynamic stability and cooling performance in pilot- or larger-scale systems. This study was to evaluate the dynamic stability or service life and cooling storage performance of a novel PCM nano-emulsion for room air-conditioning application in a self-designed, pilot-scale latent heat thermal energy storage unit. The pilot unit was constructed with a chiller, a storage tank, three sets of ceiling panels, circulation pumps and flow control valves in a pipeline. The PCM nano-emulsion remained stable through 45 repeated charging and discharging cycles over a period of 70 days in the pilot unit and could be well regenerated for even longer period of operation. The PCM nano-emulsion retained a stable cooling capacity, e.g. with a discharging rate of 199.6 W in the 1^{st}-5^{th} cycles and 196.9 W in the 35^{th}-40^{th} cycles at a given flow rate. The droplet size increased to a maximum of ~180 nm but was still small compared with many of the previously published ranges. Therefore, it is expected that the novel PCM nano-emulsion can have a long service life. Moreover, its volumetric thermal storage capacity was about 1.45 times higher than water in the range of 5.5-20 ℃, with the highest average charging rate of about 1.4 kW during the phase transition process, and a high efficiency of ~85% in the cooling energy release with no limitation by fast discharging flow rate, which make it favourable for practical situations.

Keywords: PCM nano-emulsion; Cooling energy storage; Dynamic stability; Service life; Charging and discharging rate; Pilot study.

Nomenclature <eliminate all those only used locally, e.g. variables in equations)

E_V	volumetric thermal storage capacity, J/m^3
q	charging/discharging rate, W
T	temperature, ℃
ΔT	temperature difference, ℃
$\dot{V}$	volumetric flow rate, m^3/s

v	velocity, m/s
τ	time, s
Subscripts	
avg	average
c	charging
d	discharging
E	emulsion
e	end
f	freezing
i	initial
in	inlet
m	melting
out	outlet
w	water
Abbreviations	
DAQ	data acquisition
DSC	differential scanning calorimetry
LHTES	latent heat thermal energy storage
PCM	phase change material
PCME	phase change material emulsion
PCMNE	phase change material nano-emulsion
PIT	phase inversion point
RTD	resistive temperature detector
SHS	sensible heat storage
TES	thermal energy storage

1. Introduction

Latent heat thermal energy storage (LHTES) using phase change materials (PCM) is one of the most favourable TES technologies with the potential advantages of high thermal storage capacity, long durability, and flexible working temperature compared to the sensible heat storage (SHS) or thermochemical energy storage systems [1, 2]. However, the heat transfer of a LHTES system is limited by the low thermal conductivity of PCM (0.2-0.4 W/m·K). Although the extended surface with fins of various geometrics, e.g. Y-shaped [3] or rectangular [4], is an option, the complexity of system configuration is significantly increased. Therefore, manipulation and optimization of the PCM properties is a simpler and more feasible approach such as by the addition of highly thermal conductive materials, carbon-based (graphene [6],

carbon nanotube [7], expanded graphite [8, 9], and graphite nanoparticle [10]) and metallic (nano copper [11], magnesium particle [12], nano magnetite [13], copper foam [14], and nickel foam [15]). However, heat transfer enhancement in a LHTES system using composite PCMs cannot ensure a high storage capacity. Fang et al. [16] have shown based on experiments that the effective storage capacity of a LHTES unit using an expanded graphite-PCM (20 W/m·K) was barely equivalent to that of the ideal stratified water storage tank when the heat transfer fluid flowed quickly, indicating the dramatic reduction of storage capacity with rapid energy release.

Latent functionally thermal fluids, i.e. PCM emulsions (PCMEs) [17] have been developed by dispersing PCM into a carrier fluid (e.g. water) as heat transfer and thermal storage media simultaneously, which could acquire efficient heat transfer, relatively high effective storage capacity with fast energy release, lower pumping power consumption in comparison to water, and simple system configuration. Because the PCMEs are thermodynamically unstable and phase separation occurs within a short time, considerable effort has been made to improve the stability of PCMEs. Reduction of the droplet size, especially the formation of PCM nano-emulsions (PCMNEs), could greatly enhance the stability [18]. In our recent study [19], a novel and highly stable PCMNE with an average droplet size of 57.2 nm was fabricated by the phase inversion temperature (PIT) method using n-hexadecane as the PCM ingredient and a two-surfactant mixture at an optimal composition. This PCMNE was also tested in the glass bottle for 300 melting-freezing cycles showing little change in the droplet size. However, most previous studies on the stability evaluation were only performed under static conditions, such as long-term storage at room temperature or statically repeated thermal cycles. The dynamic study of PCMNE under practical conditions has rarely been assessed.

While the flow and heat transfer characteristics of PCMEs in the tube have been widely evaluated in laminar [20, 21] or turbulent flow regime [22], there are still few or no studies on their cooling storage applications. Cao et al. [25] have recently reported the use of 10 wt% PCME with average droplet size of around 350 nm as a cooling fluid for active battery thermal

management system to achieve a lower surface temperature and temperature difference than with water. A later work from the same group [26] used 20 wt% PCME for photovoltaic module cooling, achieving a further temperature reduction by 5.3% compared with water. Liu et al. [27] have reported a lab-scale LHTES system for room cooling by applying 20 wt% PCMNE (the average droplet size at around 80 nm) as the cooling fluid, achieving a storage capacity 1.5 times higher than that of water and about 80% efficiency in cooling energy release. However, the dynamic stability or service time of PCMEs or PCMNEs was not evaluated in these studies. Moreover, to the best of our knowledge, there are only a few published studies on the performance of PCMEs in pilot- or larger-scale systems. Delgado et al. [28, 29] studied the storage capacity and heat transfer characteristics such as overall heat transfer coefficient of PCME, but it was only retained in a 46 L storage tank instead of a flow system. Biedenbach et al. [30] also investigated PCME in a 500 L storage tank for 6 days. None of these studies attempted the reuse of PCMEs after regeneration.

Based on the above literature review, there is still insufficient knowledge of the dynamic stability and cooling storage performance of PCMNEs in pilot- and large-scale TES systems. To fill this knowledge gap, this study was carried out to evaluate the dynamic stability or service life and cooling performance of a novel PCMNE for room air-conditioning application in a self-designed pilot-scale LHTES unit with regeneration capability. The novel PCMNE with an average droplet size of 78.9 nm was prepared with n-hexadecane as the PCM agent and a binary surfactant mixture plus a nucleating agent. The pilot LHTES unit was constructed with a 56 L storage tank, a chiller, a few ceiling panels, and the circulation pipeline consisting of circulation pumps and automatic flow control valves. The pilot experiments were carried out at various flow rates of the PCMNE for repeated charging and discharging cycles. Several storage performance parameters of the PCMNE were quantified and its capability for regeneration and reuse was also assessed.

2. Experimental

2.1. Materials

Alkanes, n-hexadecane ($C_{16}H_{34}$, 99%) as the PCM and n-octacosane ($C_{28}H_{58}$, 98%) as the

nucleating agent, were purchased from TCI (Tokyo Chemical Industry Co., Japan). Nonionic surfactants polyethylene glycol dodecyl ether (Brij L4) and polyoxyethylene sorbitan monostearate (Tween 60) were from Sigma-Aldrich (USA) and Macklin (China), respectively. Sodium chloride (NaCl, 99.5%) was from Aladdin. All chemicals were used as received from the suppliers.

2.2. Preparation and characterization of PCM nano-emulsion

The PCMNE was prepared by the PIT method according to the protocol as reported previously [19] with slight modifications. It consisted of 20 wt% n-hexadecane, 9.5 wt% of a surfactant mixture of Brij L4 and Tween 60 at 6:3.5 mass ratio and 2 wt% n-octacosane. The preparation procedure was quite simple including three major steps, (i) mixing n-hexadecane and surfactants on a magnetic stirrer at 400 rpm and 60 ℃; (ii) adding distilled water to the mixture; (iii) cooling the coarse emulsion rapidly to 25 ℃. A total volume of 55 L PCMNE was prepared from repeated single preparations at 1 L each due to the limited cooling ability in the laboratory since the cooling speed had a significant effect on the droplet size (to be further explained later in Section 3.3). The production of PCMNE could be easily scaled up in a mixing tank facilitated with efficient cooling.

The average droplet size of PCMNE was measured by dynamic laser scattering (Malvern Zetasizer Nano ZS). The thermal properties including latent heat and melting/freezing point were determined with a differential scanning calorimeter (Mettler Toledo, DSC3) at a heating/cooling rate of 5 ℃/min. The apparent viscosity was measured with a rotational viscometer using the ultra-low viscosity adapter (Brookfield, DV3T). The PIT point was determined by the electrical conductivity measurement [31]. For prolonged static stability evaluation, a small volume of PCMNE was filled in a 10 mL glass bottle and stored at 25 ℃.

2.3. Experimental setup: the pilot LHTES unit

The pilot LHTES unit was designed and constructed to evaluate the dynamic stability and cooling performance variation of the PCMNE as the cooling storage fluid for room air-conditioning application. Fig. 1 shows the schematic diagram and photographs of the pilot LHTES unit, and Table 1 summarises the specifications and functions of the major components.

A total 55-L volume of PCMNE was used for the pilot test, which was pumped from the storage tank to the chiller for charging of cooling energy and then to the ceiling panels for discharging, acting as both heat transfer and thermal storage media. The chiller with 2.85 kW standard cooling capacity was customized with a built-in flexible pump (Pump 1) to circulate PCMNE between the chiller and the storage tank in the temperature range of 5-40 ℃. The charging flow rate was measured with a circular gear flowmeter, which had an accuracy of 0.5% in the range of 200-3000 L/h. A diaphragm metering pump (Pump 2) with an accuracy of 2% was installed to circulate PCMNE between the storage tank and the ceiling panels and to control, and measure the flow rate during discharging, which was calibrated as a function of pump speed (Supplementary data, Fig. S1).

Three ceiling panels (Panel 1-3) were installed on the top of a chamber with an internal dimension of 4.0 m (length) × 2.7 m (width) × 2.9 m (height), and PCMNE flowed through Panel 1 to Panel 2 for discharging, and Panel 3 was used as a reference. Each ceiling panel was installed with a U-shaped copper tube of 10 m long and 10 mm inside diameter and a dimension of 1240 mm (length) × 620 mm (width) × 40 mm (height). The 750-W heater was placed in the center of the chamber to attain the desired chamber temperature. Except for the ceiling panels, all the other LHTES components including the storage tank and chiller were placed outside on the roof of the chamber. The pipeline for transportation of PCMNE in the pilot unit was formed of copper pipe (inside diameter 15 mm) and covered with a 20-mm layer of foam rubber insulation, having a total length of 25 m.

A total of 23 resistance temperature detectors (RTDs) with an accuracy of 0.2 ℃ in the temperature range of -50 to 180 ℃ were used, which were connected to a data acquisition (DAQ) system for data collection for one min. Five RTDs (Fig. 2a) were attached to the surface of each ceiling panel, which were covered by a layer of high-density polyurethane foam to reduce the influence of high chamber temperature on the measurement.

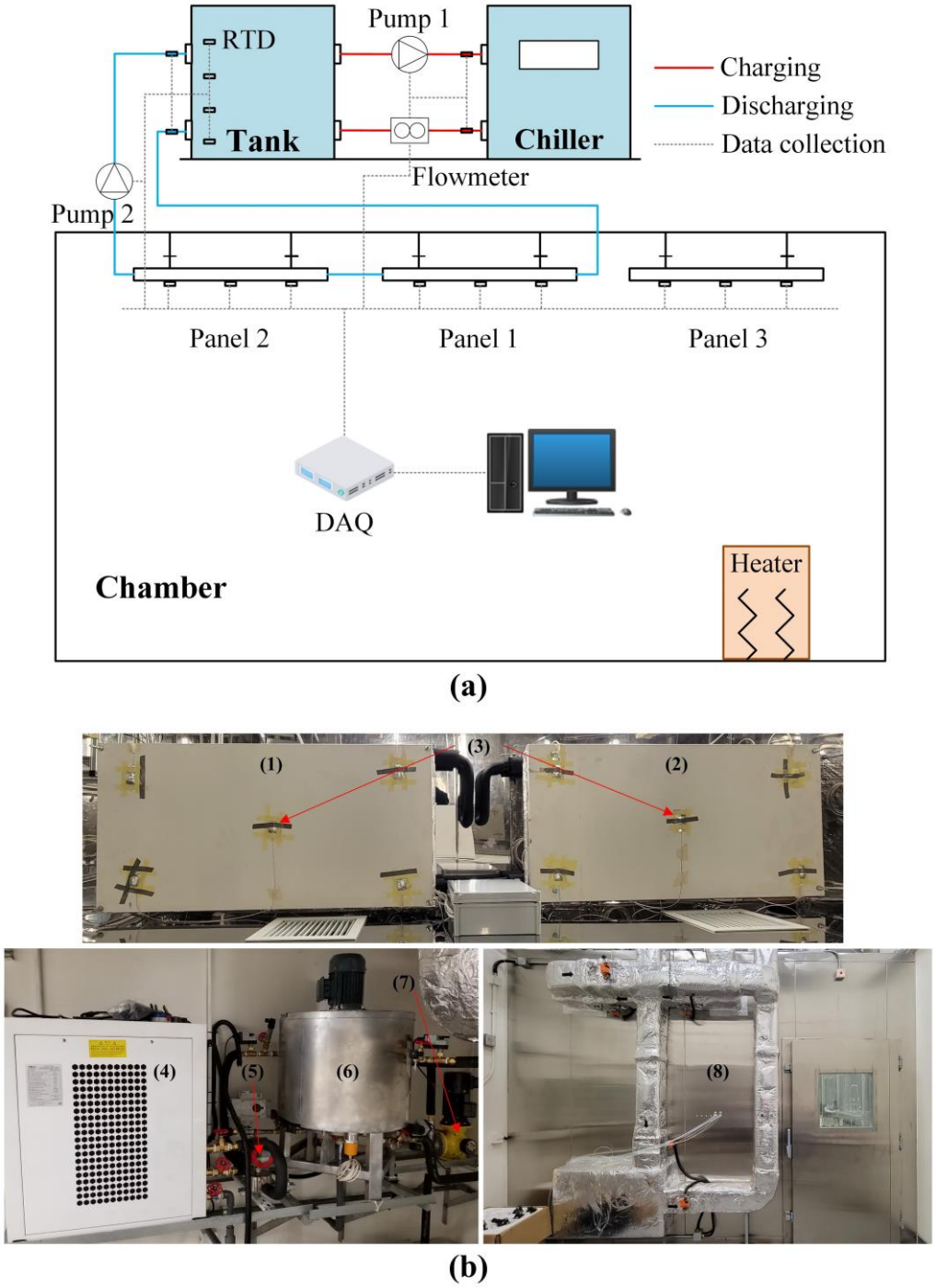

Fig. 1 Illustration of the pilot LHTES unit: (a) the schematic diagram; (b) photographs of the major components: (1) ceiling panel 1 (Panel 1); (2) ceiling panel 2 (Panel 2); (3) RTDs; (4) chiller with built-in flexible pump (Pump 1); (5) circular gear flowmeter; (6) storage tank; (7) diaphragm metering pump (Pump 2); (8) chamber.

Table 1 The specifications and functions of the major components of pilot LHTES unit.

Component	Information	Specification/function
Storage tank	Self-designed	a) Max heating temperature: 60 ℃ b) Stirring: 0-1000 rpm/min c) Internal volume: 56 L d) Storage and regeneration of PCMNE
Chiller	Customized	a) Standard cooling capacity: 2.85 kW b) Temperature range: 5-40 ℃ c) Evaporative tank volume: 17 L d) Cooling PCMNE
Flexible pump	RXB-20, Yaquan Pumps	a) Operating flow rate: 10-15 L/min b) Circulating PCMNE during charging c) Installing inside the chiller
Circular gear flowmeter	GF series, XCON Technology	a) Charging flow rate measurement b) Range:200-3000 L/h c) Accurate: 0.5%
Metering pump	GM series, Nanfang Pumps	a) Max flow rate: 85 L/h b) Accurate: 2% c) Flow rate control and measurement d) Circulating PCMNE during discharging
Ceiling panel	SAS330, SAS International	a) Discharging unit b) 10 m copper tube inside (d = 10 mm) c) Dimension: 1240 × 620 × 40 (mm)
RTD	T-type	a) Accuracy: 0.2 ℃ b) Temperature measurement
DAQ system	Trend IQ4E, Honeywell	a) Accuracy: 0.01 ℃ b) Data collection

Fig. 2b shows the detailed geometries of the storage tank, which was a cylindrical container with an internal dimension of 400 mm diameter × 450 mm height, made of stainless steel (No. 304) of 1 mm wall thickness. The stainless wall was surrounded with a built-in thermal oil jacket (5 mm thickness) which was heated with a resistance wire for PCMNE regeneration, and a 4.5-mm out layer of thermal insulation. The total volume of PCMNE in the storage tank was about 44 L, leaving a 95-mm head space between the PCMNE surface and the top cover of the storage tank. Four RTDs (T_1-T_4) were immersed into PCMNE from the top

to the bottom for temperature measurement, and another four RTDs were attached to the surface of copper pipe inside the thermal insulation to detect inlet and outlet temperature during charging and discharging. The two RTDs for charging were placed adjacent to the chiller, while the two RTDs for discharging placed about 0.2 m away from the storage tank inlet and outlet. The PCMNE was agitated with an overhead stirrer to obtain a uniform temperature throughout the storage tank either for the PCMNE regeneration or after discharging.

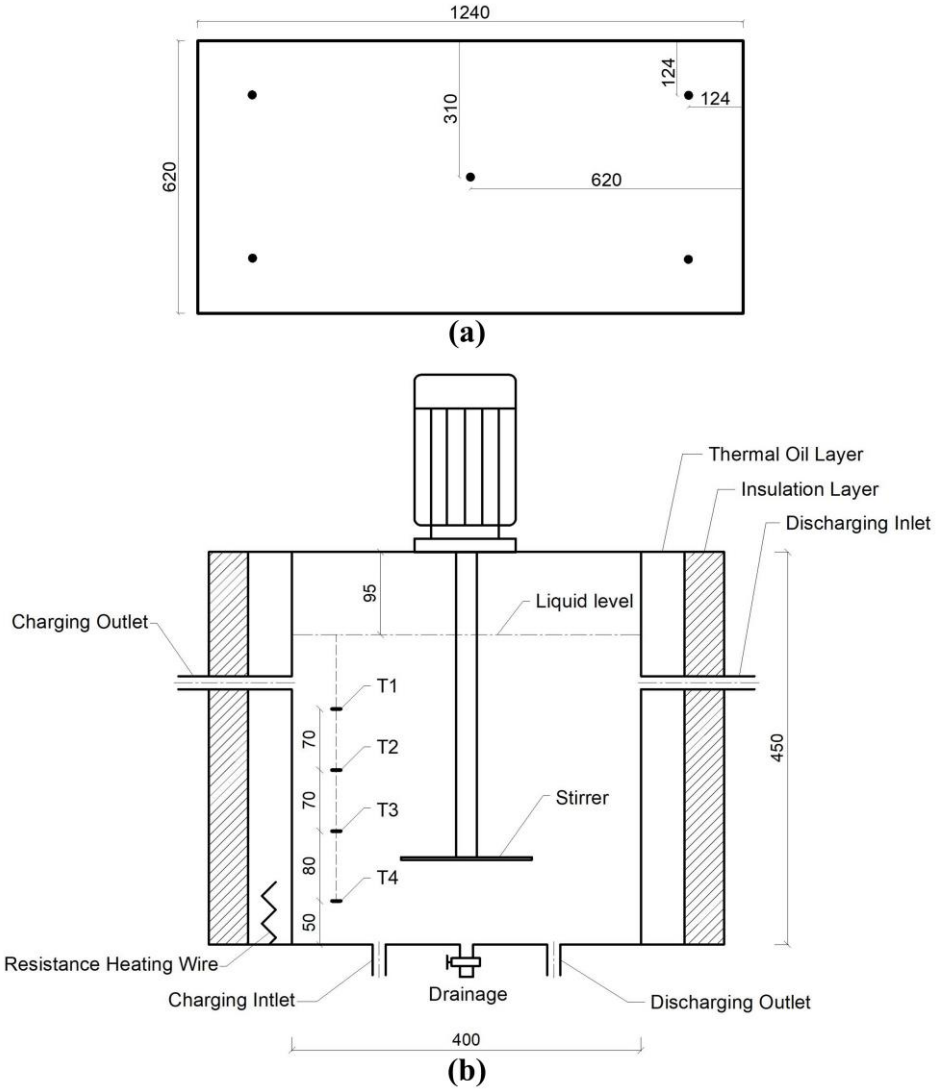

Fig. 2 Detailed diagrams of: (a) locations of five RTDs locations at the surface of ceiling panel; (b) the storage tank. (Unit: mm)

2.4. Testing conditions for the pilot LHTES unit

Preliminary tests were performed with tap water on the pilot unit. The water was firstly

cooled to 5.4 ℃, and kept for 5 h, during which the laboratory temperature was around 23.0 ℃, and the water temperature was raised to 8.2 ℃. With the results, the total thermal resistance of the tank (R_t) was estimated as 0.57 ℃/W by the following equation [32],

$$R_t = \frac{\left(T_{lab,avg} - T_{t,avg}\right)\tau}{Q_{t,loss}} = \frac{\left(T_{lab,avg} - T_{t,avg}\right)\tau}{m_w C_{p,w}\left(T_{e,w} - T_{i,w}\right)} \quad (1)$$

where $T_{lab,avg}$ and $T_{t,avg}$ are the average temperature of the laboratory and that of the storage tank during τ period, m_w and $C_{p,w}$ the mass and specific heat capacity of water, $T_{i,w}$ and $T_{e,w}$ the initial and final water temperature in the storage tank, respectively. Water was then circulated between the storage tank and the chiller with cooling and heating in the range of 5.5-20 ℃, from which the cooling and heating curve of water were derived for comparison with those of PCMNE.

The charging performance test was performed at the maximal circulation flow rate of flexible pump for rapid charging study, while the discharging performance through the ceiling panels (Panel 1-2) in the chamber was evaluated at different flow rates. The preliminary results showed that too high a discharging flow rate of water would lead to a higher surface temperature of ceiling panels with the constant heat load in the chamber, which would cause a weaker cooling capacity. Because of practical considerations such as the higher heat capacity of PCMNE and the limited heat load (750 W) in the chamber, only two discharging flow rates (0.154 and 0.194 L/min) were selected for the comparison of discharging performance between water and PCMNE. The total discharging times were around 230 and 280 min, respectively, implying that about 44 L cooled water could be withdrawn from the storage tank. Prior to discharging, the heater was switched on (80 and 100 min for 0.154 and 0.194 L/min, respectively) to raise the chamber temperature, and was kept on during the whole discharging period to maintain the discharging outlet temperature bigger than 18 ℃, indicating the full cooling energy release through ceiling panels.

After the preliminary tests, water was withdrawn from the pilot unit and replaced with PCMNE (total volume 55 L). Because of a small volume of water remaining in the pipeline and ceiling panels, the total liquid volume was about 60 L (44 L in the storage tank, 10 L in the

chiller, and 6 L in the pipeline and ceiling panels), so that the PCMNE was diluted by tap water about 9% (v/v). The PCMNE was retained in the pilot unit for 45 charging-discharging cycles, where each complete charging-discharging cycle was defined as the charging or cooling by the chiller to ~5.5 ℃ and then discharging by Panel 1-2 to ~20 ℃. The droplet size and thermal properties of PCMNE were determined for every 5 cycles. In addition, the discharging performance of PCMNE through Panel 1-2 was tested and compared during the 1st-5th and 35th-40th cycles in the same testing conditions as for water in the preliminary tests. The test at each condition (e.g. flow rate) was performed at least twice with both water and PCMNE.

2.5. Estimation of LHTES performance

A few of the major LHTES performance parameters were derived from the test results including average charging/discharging rates, volumetric thermal storage capacity, and surface temperature of ceiling panels. The average charging or discharging rate can be calculated by,

$$q_{avg} = \frac{\Delta Q}{\tau} \tag{2}$$

where ΔQ is the energy change in the storage tank during τ period. For water, ΔQ_w equals to the change of sensible heat $m_w C_{p,w} \Delta T_w$, while for PCMNE, ΔQ_E, the latent heat change is added as $m_E C_{p,E} \Delta T_E + \Delta H$. The volumetric thermal storage capacity of charging ($E_{V,c}$) and discharging ($E_{V,d}$) are given by the following equations,

$$E_{V,c} = \frac{\Delta Q}{V} \tag{3}$$

$$E_{V,d} = \frac{\Delta Q - Q_{t,loss}}{V} \tag{4}$$

where V is the volume of water or PCMNE in the storage tank. The surface temperature of ceiling panels (T_s) can be estimated by [33]:

$$T_s \approx T_{min} + 0.5(T_{max} - T_{min}) \tag{5}$$

where T_{min} and T_{max} are minimum and maximum surface temperature of ceiling panels.

2.6. Estimation of pumping power

The pressure drop (ΔP) and pumping power (P_p) can be estimated by the following equations [18] (considering only the skin frictional loss in the pipeline),

$$\Delta P = f\frac{L}{2d}\rho v^2 \quad (6)$$

$$P_p = \frac{\dot{V}\Delta P}{\eta} \quad (7)$$

where L and d are the length and inside diameter of copper tube, respectively, ρ the fluid density, v the fluid velocity, $\dot{V}$ the volumetric flow rate, and η the pump efficiency; f is the Fanning friction factor estimated by (for laminar flow) [34],

$$f = \frac{16}{Re} \quad (8)$$

$$Re = \frac{\rho v d}{\mu} \quad (9)$$

where τ is the fluid viscosity. From Eqs. (6) - (10), the pressure drop and pumping power can be estimated by,

$$\Delta P = \frac{8\mu L v}{d^2} \quad (10)$$

$$P_p = \frac{8\mu L v \dot{V}}{\eta} \quad (11)$$

3. Results and discussion

3.1. Static characteristics of PCM nano-emulsion

Fig. 3 shows the characteristics of the novel PCMNE with 20 wt% n-hexadecane during the storage period at 25 ℃ for 9-15 months. As seen from Fig. 3a, the droplet size distribution (volume%) showed a gradual shift to right or the increase of droplet size with the increasing storage period. The photographs of PCMNE showed the change from a bluish translucent appearance upon preparation to a milky white color after 9 and 15 months with the increase in droplet size. As shown in Table 2, the average droplet size increased from 78.9 nm initially to 107.2 nm after 15 months, demonstrating an excellent static stability.

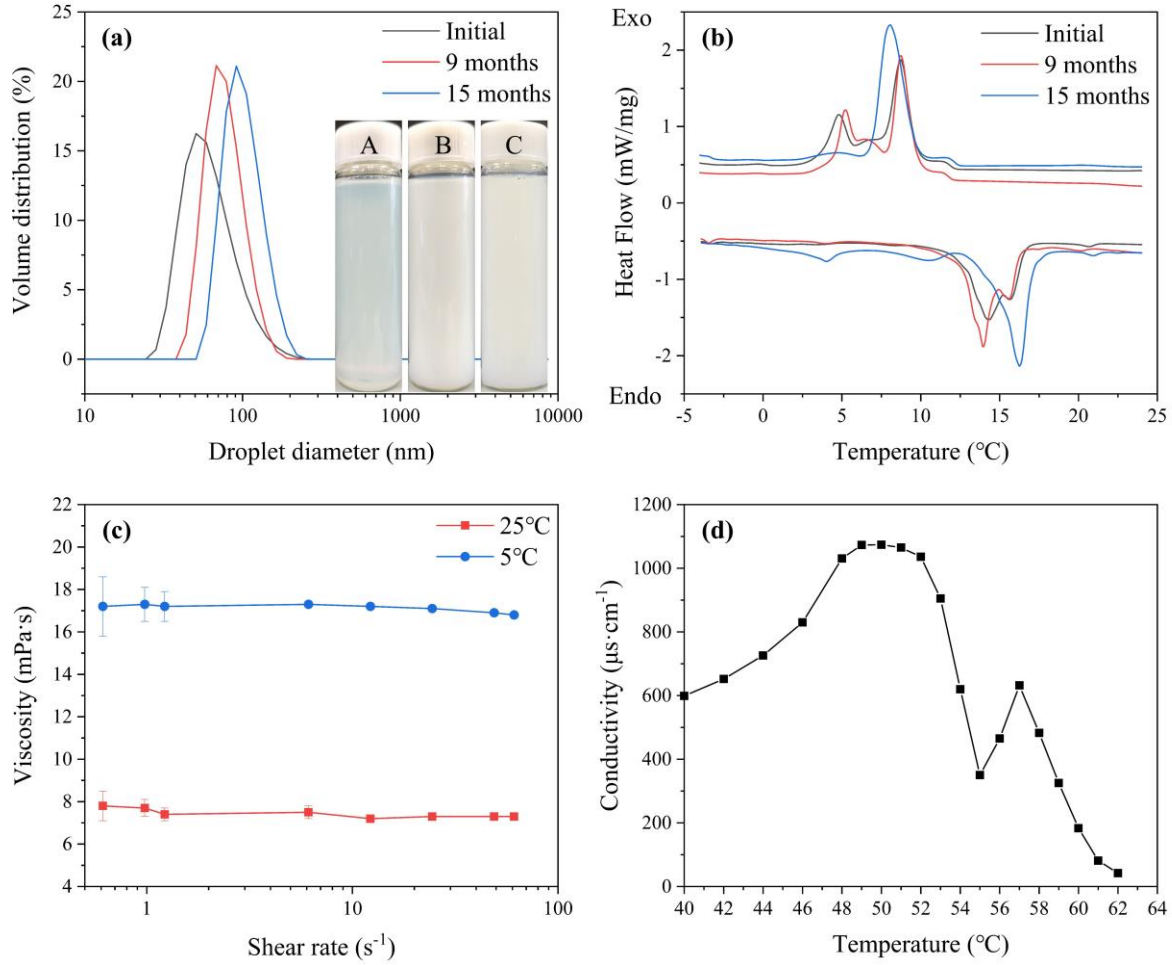

Fig. 3 Characteristics of 20 wt% PCMNE: (a) droplet size distribution (volume%) upon preparation, and after 9 and 15 months, with the inserted corresponding photographs as A, B and C, respectively; (b) DSC curves; (c) apparent viscosity-shear rate curves; (d) electrical conductivity-temperature curve.

As seen from the DSC curves (Fig. 3b), the thermal properties of PCMNE remained almost unchanged after 9 months. After 15 months, however, the melting curve exhibited an obvious shift with a higher onset melting point of 14.6 ℃(Table 2). The latent heat of the main melting peak decreased to 37.7 J/g since a minor melting peak appeared at around 5 ℃with the latent heat of 3.3 J/g, which is abnormal.

As shown by Fig. 3c, the PCMNE behaved like a Newtonian fluid with a relative constant apparent viscosity at varying shear rate. The apparent viscosity increased from ~7.5 mPa·s at 25 ℃to ~17 mPa·s at 5 ℃, ensuring a good fluidity and a low pumping power consumption.

From the electrical conductivity-temperature curve (Fig. 3d), the PIT point of PCMNE was estimated as 58 ℃, between 53 ℃62 ℃with a sudden drop of electrical conductivity. With this value, the PCMNE can be easily regenerated by heating to over the PIT point followed by quick cooling.

Table 2 The average droplet size and thermal properties of 20 wt% PCMNE.

Samples	Size (nm)	ΔH_m (J/g)	ΔH_f (J/g)	Onset T_m (℃)	Onset T_f (℃)
Initial	78.9	-41.2	42.3	12.8	10.0
9 months	86.7	-40.3	42.6	12.4	9.9
15 months	107.2	-37.7	42.8	14.6	9.8

3.2. Dynamic characteristics of PCM nano-emulsion

The 55-L PCMNE was then tested in the pilot LHTES unit for 45 complete cycles over 70 days and Fig. 4 shows the properties recorded during the pilot test. As shown in Fig. 4a, the average droplet size increased gradually in the first 25 cycles to the maximum of ~180 nm and only varied slightly in the following cycles, which was very interesting. For better explanation for this trend, the droplet size distribution (intensity%) was plotted in Fig. 4b, where an initial single peak of size distribution turned to a bimodal curve with another peak around 300 nm after 10 cycles, implying the formation of large droplets due to coalescence. Since the coalescence is governed by the collision frequency, it mainly occurred during charging process as PCMNE flowed in turbulent region. The peak intensity in the large droplet size range was dramatically increased after 25 cycles, indicating the continuous growth of the large droplet proportion and in turn, the growth of average droplet size. Although the peak intensity slightly grew after 35 cycles, the large peak value decreased to around 260 nm, and decreased further to around 230 nm after 45 cycles, turning to a unimodal size distribution again. In this way, the average droplet size fluctuated at ~180 nm during 25-45 cycles. Based on the above results, it is predicted that the PCMNE after 45 cycles could be used for many more cycles because the average droplet size was still lower than the value reported by most previous studies.

As seen from the DSC melting curves (Fig. 4c), a small melting peak with an onset melting point at ~17 ℃ appeared after 5 cycles and its area gradually increased till the 25th cycle, indicating a shift of the main melting point. Interestingly, the melting peak shift with the cycles had some similarity to that of the droplet size, suggesting a possible relationship between the droplet size and the melting point. As observed in our previous studies, the onset melting point of the n-hexadecane nano-emulsion with a droplet size around 100 nm was ~12.5 ℃ [19, 35], and turned to ~17 ℃ as the emulsion droplet size increased to 400 nm [36] which was equal to that of bulk n-hexadecane. The melting point trend suggests that only when the droplet size is below a critical dimension, will the onset melting point of n-hexadecane decrease significantly.

As shown in Fig. 4d, the DSC freezing curve of PCMNE initially had two peaks but turned to a single peak at a lower onset freezing point temperature of 7.5 ℃ after 5 cycles, which then remained at 5-6 ℃ in the following cycles. It is noteworthy that the onset freezing point measured by DSC could be different from that obtained from the chiller since only a few milligrams of PCMNE was used for the DSC measurement. In particular, the onset freezing temperature was about 5 ℃ at the 45th cycle, implying that PCMNE could not store any latent heat if cooled by the chiller to 5.5 ℃. However, this was not true to the actual situation as discussed in Section 3.4.1. Owing to the great complexity of supercooling with the PCME in the chiller [37], the present study ignored the supercooling issue, assuming a full crystallization of nano-droplets cooled by the chiller. Because of the dilution factor by water, the melting and freezing latent heat of PCMNE were about 34 and 37 J/g, respectively (Supplementary data, Table S1). However, there was no trend of latent heat reduction after 45 cycles. Other important properties of PCMNE in the pilot unit were density and specific heat capacity, 970 kg/m^3 and 3.7 kJ/(kg·℃), respectively.

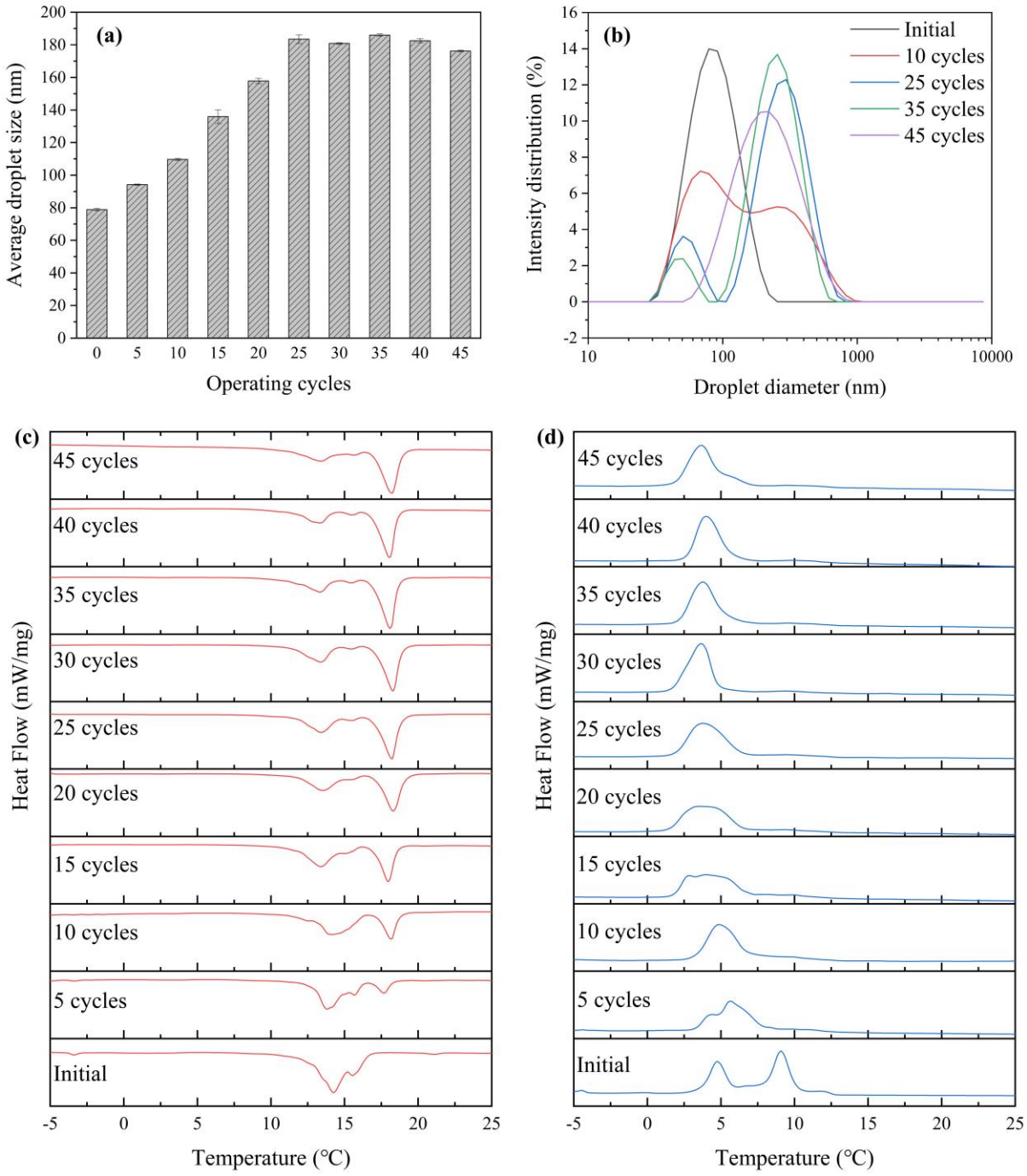

Fig. 4 Changes of PCMNE properties through 45 cycles in the pilot LHTES unit: (a) the average droplet size; (b) droplet size distribution (intensity%); (c) DSC melting curves; (d) DSC freezing curves.

3.3. Regeneration characteristics of PCM nano-emulsion

After 45 cycles in the pilot LHTES unit, the 60 L PCMNE (with ~5 L tap water) was regenerated by heating to over 58 ℃, followed by quick cooling to 25 ℃. As shown in Fig. 5,

the regenerated PCMNE exhibited a Newtonian-flow behavior at 5 ℃ and 25 ℃ because of relatively stable apparent viscosities as the increasing shear rate (Fig. 5a). The viscosity was ~5 mPa·s at 25 ℃ and increased to ~11 mPa·s at 5 ℃. It is worthy to note that PCMNE after 45 cycles exhibited a shear thinning property of a pseudoplastic fluid at 5 ℃, probably relating to the droplet size increase. The average droplet size and thermal properties of the regenerated PCMNE were nearly identical to those of the initial PCMNE, as showing in Fig. 5b-c. The photographs of PCMNE after 45 cycles and regeneration were presented in Fig. S2 (Supplementary data), demonstrating the high stability.

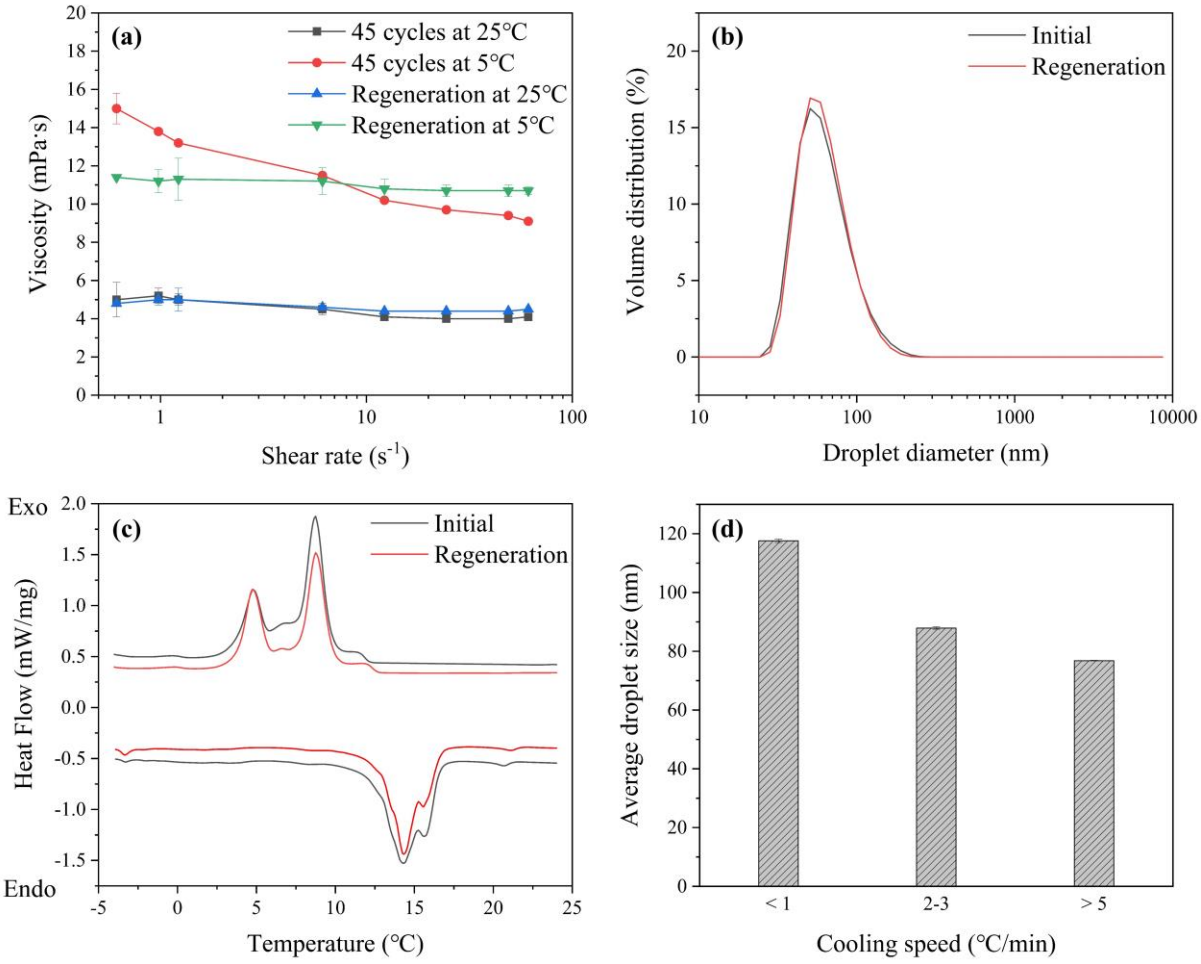

Fig. 5 Characteristics of regenerated PCMNE: (a) apparent viscosity-shear rate curves; (b) droplet size distribution (volume%); (c) DSC curves; (d) the average droplet size with different cooling speed.

It is noteworthy that PCMNE diluted by tap water was still stable and could be regenerated,

and this robustness is favourable for practical applications. On the other hand, PCMNE could only be fully regenerated with the average droplet size of 76.8 nm by quick cooling (> 5 ℃/min). To achieve such a high cooling speed in the pilot unit for regeneration was not feasible, since the current chiller could only achieve a cooling speed of 0.5 ℃/min. If the thermal inertia of thermal oil jacket were considered, the cooling speed would be even lower for the regeneration. Under this circumstance, Fig. 5d shows the effect of cooling speed on the average droplet size. With a cooling speed of 0.7 ℃/min, PCMNE could be partially regenerated with the average droplet size of 117.6 nm. As the cooling speed was increased to 2-3 ℃/min, the average droplet size was decreased to 87.9 nm, close to the initial value. Therefore, PCMNE regeneration in this study was conducted in the lab with a single production volume of 1 L. A feasible improvement of the current pilot unit is to add another chiller and pump to circulate and cool thermal oil in the built-in jacket after the heating process. In this way, the quick cooling speed in the pilot unit can regenerate the PCMNE to the desirable properties.

3.4. LHTES performance of PCM nano-emulsion in comparison with water

3.4.1. Charging process

Fig. 6 shows the heating and cooling curves in the storage tank with either PCMNE or water as the fluid. As shown in Fig. 6a, in the cooling period, the initial PCMNE was gradually cooled down with a linear temperature from 20 to about 12 ℃, and then experienced a notable slowdown of temperature decrease in the range of 11-12 ℃, the onset freezing temperature of PCMNE, which was slightly higher than the value (~10 ℃) obtained from DSC. During heating, the melting temperature range of PCMNE was 12-15 ℃, which was fairly consistent with the DSC result. In both cooling and heating period, the temperature gradient (T_1-T_4) in the storage tank was negligible due to a relatively high circulation flow rate (10-15 L/min). After 45 cycles (Fig. 6b), PCMNE had a smooth cooling curve and an obvious slowdown of temperature increase in the range of 16-17 ℃ in the heating period, indicating the shift of melting peak as mentioned in the above DSC section. More importantly, it proved that latent heat could be still stored in PCMNE in the 45th cycle.

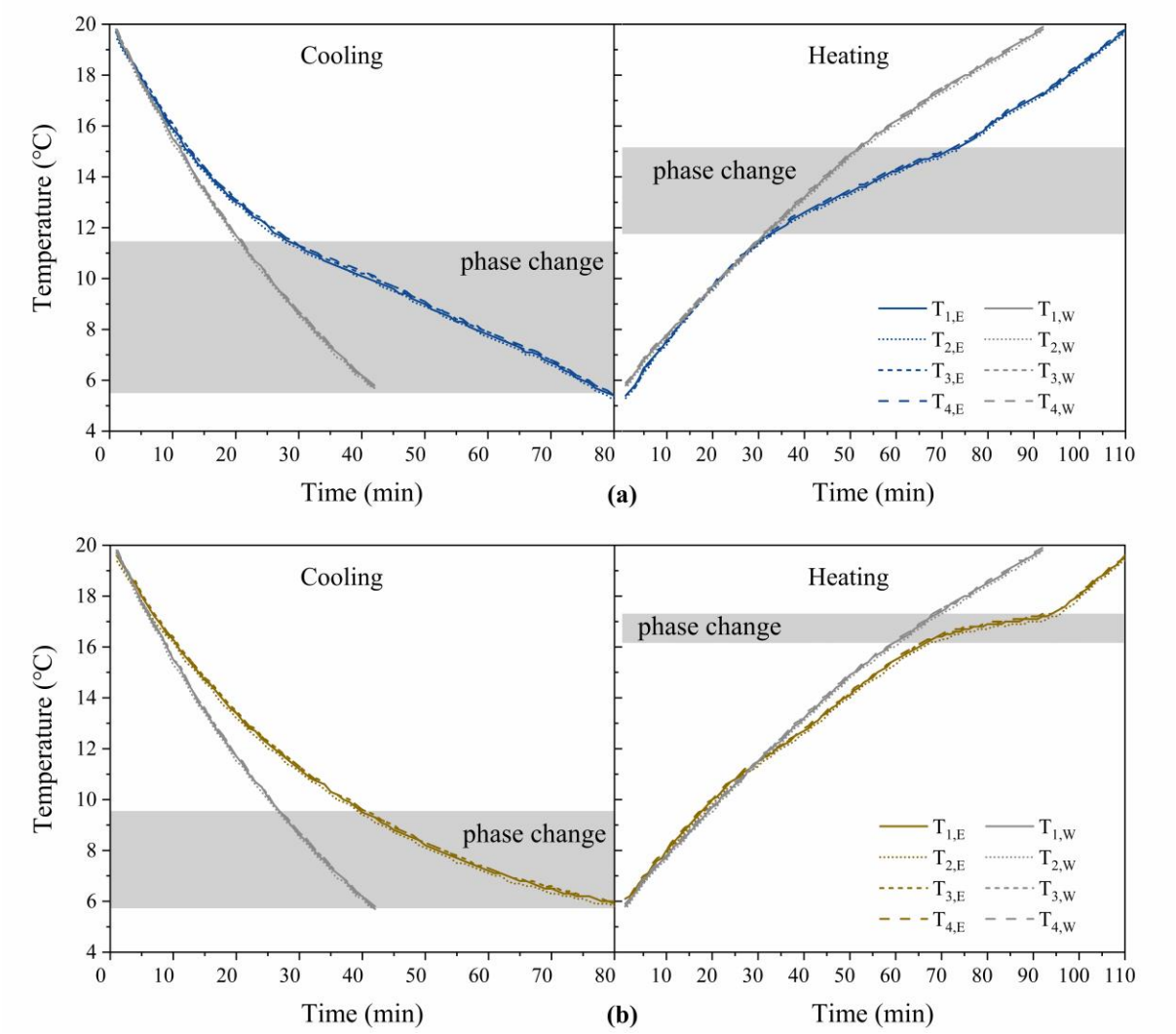

Fig. 6 Heating and cooling curves in the storage tank with PCMNE or water, which was circulated between the storage tank and the chiller with cooling and heating in the range of 5.5-20 ℃: (a) initial PCMNE; (b) PCMNE at the 45th cycle.

Since it was hard to directly obtain the onset freezing point from the cooling curve of PCMNE after 45 cycles, the difference in the cooling time between PCMNE and water was plotted against the cooling temperature and analysed as shown in Fig. 7. The crystallization of PCM led to the continuous increase in the time required for PCMNE to achieve the same temperature as water. With the initial PCMNE (Fig. 7a), the time difference was increased steadily at a maximum slope starting from 11.7 ℃, consisting with the notable slowdown observed in Fig. 6a. After 45 cycles (Fig. 7b), PCMNE had an onset freezing temperature of 9.5 ℃, which was much higher than the result detected by DSC, indicating the different

supercooling characteristics between DSC and the equipment, i.e. chiller.

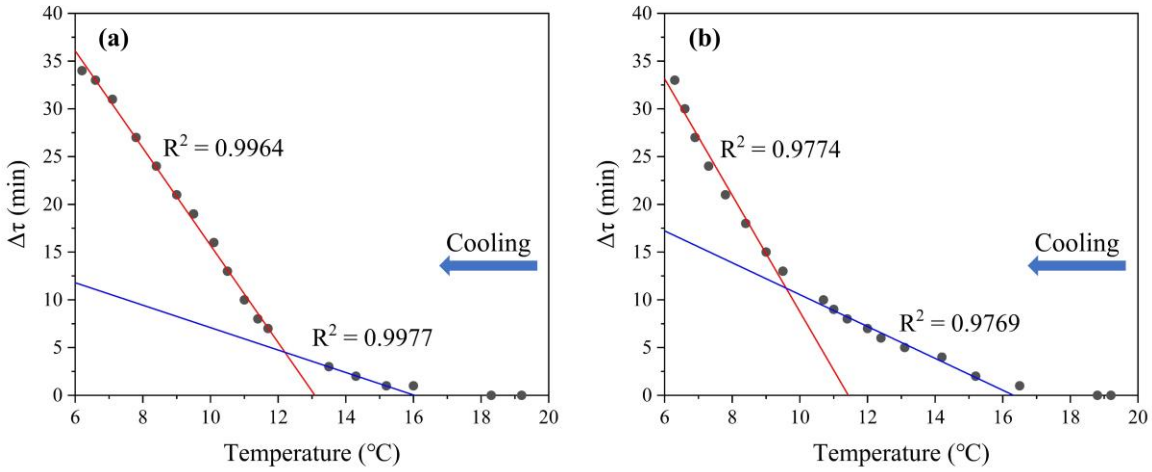

Fig. 7 The cooling time difference between PCMNE and water to the same cooling temperature: (a) initial PCMNE; (b) PCMNE at the 45th cycle.

Table 3 Summaries of the charging performance parameters of PCMNE and water.

Cycle	T_i (℃)	T_e (℃)	τ (min)	$E_{V,c}$ (MJ/m^3)	$q_{c,avg}$ (W)
PCMNE					
1st	20.0	5.5	80	87.9	806.0
3rd	20.1	5.5	81	88.3	799.3
5th	19.9	5.5	79	87.6	812.9
35th	20.0	5.5	83	87.9	776.9
38th	20.0	5.5	84	87.9	767.6
40th	19.9	5.5	83	87.6	773.7
Water					
1st	20.3	5.5	46	61.7	984.3
2nd	20.0	5.5	46	60.5	964.3
3rd	19.9	5.5	46	60.1	957.6

Table 3 shows the charging performance parameters including the average charging rate ($q_{c,avg}$) and charging volumetric thermal storage capacity ($E_{V,c}$), of PCMNE in the temperature range of 5.5-20 ℃. The average $E_{V,c}$ of PCMNE, 87.9 MJ/m^3, was 1.45 times higher than that

of water. It took 80 min to cool PCMNE from 20 to 5.5 ℃ in the first 5 cycles and only 3 min longer to achieve the same temperature decrease after 35-40 cycles. The longer cooling time in the later cycles was most probably attributed to a small drop of circulation flow rate observed during charging as a result of PCMNE property changes. Nevertheless, the changes in the properties had little effect on its charging performance in the pilot unit. Consequently, the $q_{c,avg}$ of PCMNE was initially 806.1 W and 772.8 W after 35-40 cycles, which were not too much lower than that of water as 968.7 W. This suggests that the direct transportation of PCMNE to the chiller for charging is efficient and rapid charging can be achieved.

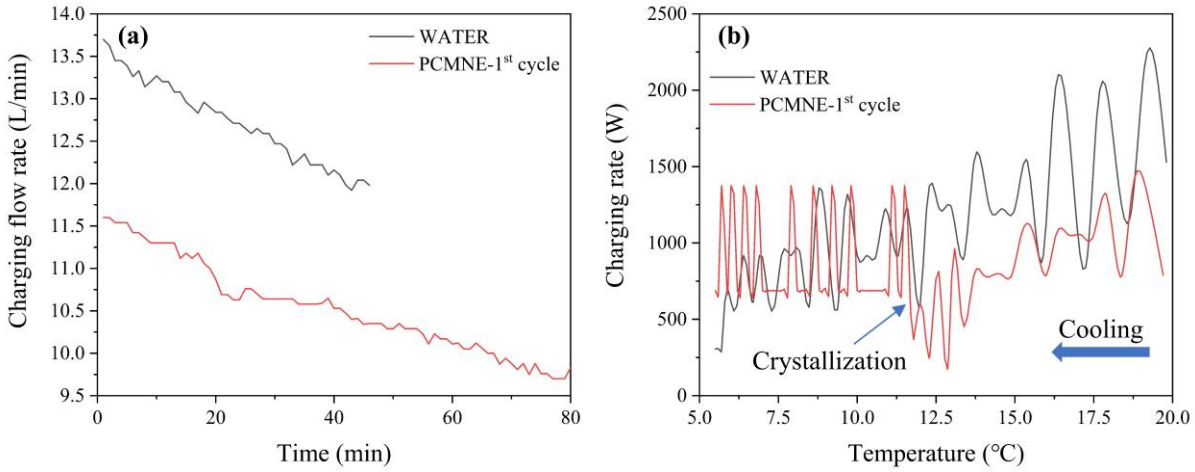

Fig. 8 The comparison between water and initial PCMNE during charging: (a) charging flow rate; (b) average charging rate per min as a function of cooling temperature.

Additionally, the difference of $q_{c,avg}$ between water and PCMNE could also be attributable to the difference in the circulation flow rate during charging, as shown in Fig.8a. The charging flow rate was gradually decreased since the increasing viscosity of water and PCMNE with the gradual temperature decrease. The average charging flow rate of water was 12.4 L/min, around 1.2 times higher than the initial flow rate of PCMNE at 10.4 L/min, which was close to the $q_{c,avg}$ difference of 1.2-fold. The $q_{c,avg}$ per min against the cooling temperature was also analysed in Fig. 8b, where only the initial PCMNE was included since the properties of PCMNE varied after the cycles. The effective specific heat capacity was adopted as $C_{p,E}+\Delta H/\Delta T$ during the phase transition process, where ΔT was 6.2 ℃ for the initial PCMNE (5.5-11.7 ℃). At the beginning of charging, the average charging rate of water could be up to

over 2 kW, and then a decreasing trend was observed. The initial PCMNE had a similar trend before the onset freezing point but $q_{c,avg}$ was much lower. Once the temperature reached to around 12 ℃, $q_{c,avg}$ increased sharply. During the phase transition process, the highest and average $q_{c,avg}$ of PCMNE were about 1.4 and 0.82 kW, respectively, which were all higher than the corresponding values of water in the range of 5.5-12 ℃. The major cause could be attributed to the enhanced heat transfer (or a higher transfer coefficient) in the evaporative tank during the phase transition process. With a low stirring speed, the overall heat transfer coefficient of PCME during melting in the storage tank was almost 2 times higher than that of water [28]. Another study has also shown a similar result during charging of MPCM slurry in a storage tank, but its overall heat transfer coefficient was almost the same as that of water without phase transition process [38].

3.4.2. Discharging process

Fig. 9 shows the temperature distribution in the storage tank during discharging at a flow rate of 0.154 L/min through the ceiling panels, that temperature increase started from the top to the bottom due to the effect of stratification. In this way, the discharging inlet temperature (T_{in}) from the bottom outlet could remain at a low level for a long discharging period, ensuring a maximum efficiency of cooling energy release. Meanwhile, the temperature distribution curves overlapped closely from the beginning to end of the cycles, indicating a negligible effect of PCMNE property changes on the discharging performance. After the whole discharging period of around 280 min, the cooled PCMNE in the storage tank was exhausted, and the overhead stirrer was switch on to ensure a uniform temperature distribution in the storage tank.

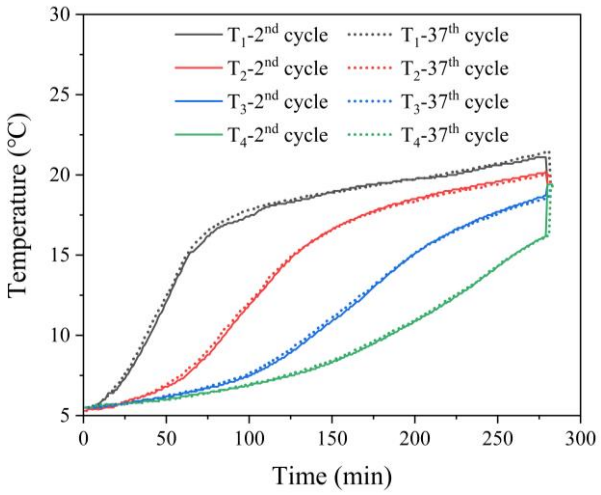

Fig. 9 Temperature distribution in the storage tank during discharging through ceiling panels with flow rate of PCMNE at 0.154 L/min.

Table 4 Summaries of the discharging performance parameters of PCMNE and water.

$\dot{V}$ (L/min)	Cycle	T_i (℃)	T_e (℃)	τ (min)	$E_{V,d}$ (MJ/m^3)	$q_{d,avg}$ (W)
PCMNE						
0.154	2nd	5.5	19.4	279	75.9	199.4
	5th	5.6	19.6	280	76.3	199.7
	37th	5.4	19.3	281	75.7	197.7
	38th	5.6	19.3	281	75.1	196.0
0.194	3rd	5.6	18.5	229	73.3	234.8
	4th	5.7	18.5	230	72.9	232.5
	35th	5.6	18.6	230	73.6	234.8
	39th	5.4	18.4	226	73.6	238.9
Water						
0.154	1st	5.4	20.9	281	58.1	151.6
	2nd	5.3	21.0	281	58.9	153.7
0.194	1st	5.4	20.7	230	58.4	186.1
	2nd	5.2	20.5	230	58.3	185.8

Table 4 summarizes the discharging performance of PCMNE versus water. In the case of

water, the average temperature increases in the storage tank (T_e - T_i) were 15.6 ℃ at 0.154 L/min and 15.3 ℃ at 0.194 L/min, respectively. This assured the effective temperature control of chamber to compare the discharging performance with the two different flow rates in the almost same temperature range. Therefore, the discharging volumetric thermal storage capacity ($E_{V,d}$) of water at 0.154 and 0.194 L/min flow rate was the same, equal to about 58 MJ/m^3, while the average discharging rate ($q_{d,avg}$) at flow rate of 0.194 L/min was higher, up to 186 W, due to a shorter discharging period. In the case of PCMNE, the average temperature increase in the storage tank at flow rate of 0.154 L/min was ~14 ℃ at the beginning and the end of each cycle, which was smaller than that of water because of a high latent heat. The negligible difference of temperature increase shows again that the droplet size change of PCMNE had little effect on the discharging performance.

As flow rate of PCMNE was increased to 0.194 L/min, the average temperature increase in the storage tank (T_e - T_i) was further decreased to ~13 ℃ (vs. ~14 ℃ at 0.154 L/min, and 15.3 ℃ for water at 0.194 L/min), reflecting a high sensitivity of the pilot unit to the flow rate change of PCMNE during discharging, due mostly to a higher heat capacity. Overall, the latent heat stored in PCMNE could be fully released at 0.194 L/min with the shift of the main melting peak. Therefore, a higher flow rate was not applied or it would give a lower efficiency of cooling energy release with the pilot unit. Although a direct comparison of $E_{V,d}$ and $q_{d,avg}$ between PCMNE and water at the same temperature range was not appropriate, the $q_{d,avg}$ value of PCMNE at 0.154 L/min was even higher than that of water at 0.194 L/min, proving a much better cooling performance. Additionally, $E_{V,d}$ of PCMNE was 73-75 MJ/m^3, accounting for a major proportion (86.2% and 83.4% for 0.154 and 0.194 L/min, respectively) of stored cooling energy during charging. The high efficiency of cooling energy release would not be affected with a high flow rate as long as the heat load was high or more ceiling panels were installed, which is the chief advantage of the direct transportation of PCMNE as the cooling fluid.

The pressure drop can be estimated by Eq. (10), where L = 25 m, d = 0.01 m and the diluted PCMNE was approximately a Newtonian fluid having a viscosity of 12 and 5 mPa·s at 5 ℃ and 25 ℃, respectively. The corresponding values for water were 1.5 and 1.0 mPa·s,

respectively. During discharging, the average viscosity of PCMNE was about 8 times higher than that of water, so that the pressure drop was also 8-fold higher at an equal velocity. On the other hand, the discharging volumetric flow rate was very small, only 0.194 L/min ($v = 4.1\times10^{-2}$ m/s), contributing to a very small pressure drop, below 1.0 kPa for PCMNE. Therefore, the pumping power difference for PCMNE and water was negligible for this pilot system, which was consistent with other reported results at low flow rates [18, 39].

Further evaluation of the cooling performance of PCMNE versus water is made with surface temperatures of ceiling panels recorded during the cycles (Fig. 10). Fig. 10a shows the two sets of temperature curves of ceiling panels in the 2nd and 5th cycles with PCMNE at flow rate of 0.154 L/min, which were highly reproducible. The surface temperature of the reference Panel 3 (T_{P3}) increased steadily from about 29.5 to 35 ℃ during the 280 min discharging period, while surface temperatures of Panel 1 and Panel 2 remained at a much lower level. Specifically, ΔT_{P1} (the surface temperature difference between Panel 1 and Panel 3) reached the maximum of 11-12 ℃ in ~30 min and about 40 min for ΔT_{P2} to reach the plateau of 9-10 ℃.

Fig. 10b offers a comparison of the temperature profiles of ceiling panels with PCMNE at two different flow rates. At the higher flow rate of 0.194 L/min (3rd cycle), T_{P3} was from 32 to 36 ℃ in 230 min of discharging, about 2 ℃ higher than that of PCMNE at 0.154 L/min (2nd cycle). The temperature plateau was about 13 ℃ for ΔT_{P1} and 11-11.5 ℃ for ΔT_{P2}. Since T_{P3} was higher at 0.194 L/min, the surface temperature of Panel 2 at 0.194 L/min was even lower than that of Panel 1 at 0.154 L/min, demonstrating a significant increase of cooling capacity at a higher flow rate. Fig. 10c-d provides a comparison of the temperature results of water and PCMNE at the beginning and end of the cycles with different flow rates. At 0.154 L/min, ΔT_{P1} of water was slightly lower (0.5 ℃) than that of PCMNE at the 2nd cycle in the first 140 min and thereafter, the difference increased gradually as a result of the faster surface temperature increase of Panel 1 with water. Moreover, a minor difference no more than 0.7 ℃ was observed after 140 min for PCMNE between the 2nd and 37th cycle, which could be attributed to the changes of PCMNE properties. For Panel 2, its cooling performance with water was limited, about 2 ℃ lower surface temperature than with PCMNE. Also, its cooling capacity with

PCMNE at the 37th cycle was slightly outperformed that at the 2nd cycle.

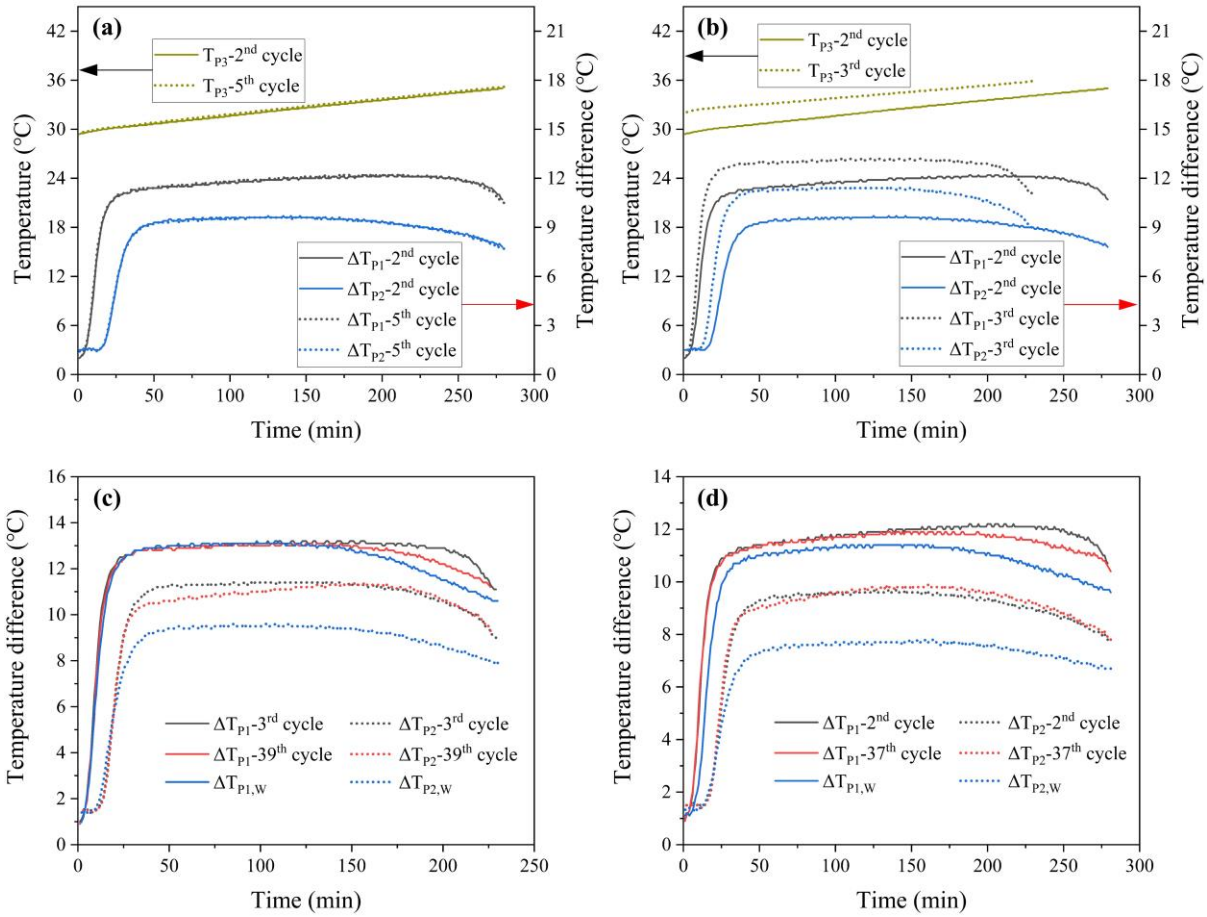

Fig. 10 The comparison of surface temperatures of ceiling panels: (a) PCMNE at 0.154 L/min; (b) PCMNE at 0.154 and 0.194 L/min; (c) PCMNE and water at 0.154 L/min; (d) PCMNE and water at 0.194 L/min. ($T_{P1\text{-}P3}$: Surface temperatures of Panel 1-3; Temperature difference $\Delta T_{P1/P2} = T_{P3} - T_{P1/P2}$)

The cooling capacity of Panel 1 was the same for both water and PCMNE in the first 150 min discharging at 0.194 L/min. Similar to the case of 0.154 L/min, the difference appeared because of a faster ΔT_{P1} decrease with water, followed by PCMNE at the 39th cycle. Interestingly, the ΔT_{P2} change of PCMNE between the 3rd and the 39th cycle also occurred at 150 min. For further analysis of the relationship between ΔT_{P1} and ΔT_{P2}, the discharging inlet and outlet temperature are presented in Fig. 11, showing that the main difference of PCMNE in the melting temperature range (T_m), shifting from 12-15 ℃ in the 3rd cycle to 16-17 ℃ in the 39th cycle.

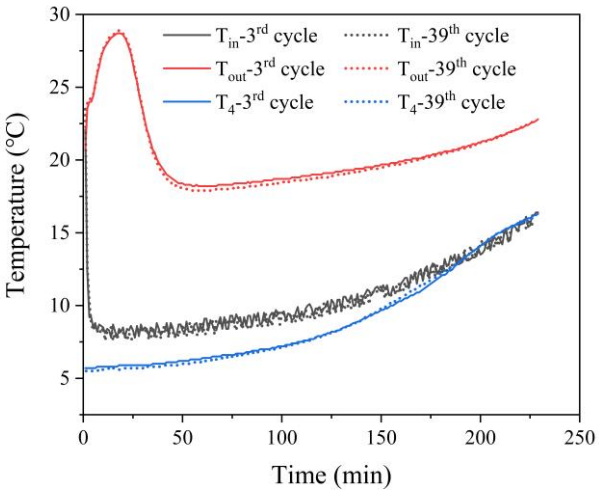

Fig. 11 The discharging inlet and outlet temperature of PCMNE at the 3rd and 39th cycles with flow rate of 0.194 L/min.

At the beginning of discharging, as the inlet temperature (T_{in}) was very low, PCMNE (T_m = 12-15 ℃) could not be fully melted in Panel 1. A larger proportion of latent heat was released in Panel 2, so that ΔT_{P2} of PCMNE (3rd cycle) was higher than that in the 39th cycle. With the increase in T_{in}, the latent heat release in Panel 2 was decreased for PCMNE in the 3rd cycle, while a small percentage of latent heat (39th cycle) could be released in Panel 2 (but not in the copper pipe connecting the storage tank and Panel 2). Therefore, the ΔT_{P2} difference was gradually decreased until ΔT_{P2} of PCMNE in the 39th cycle exceeded that in the 3rd cycle. At 150 min, T_{in} was around 10 ℃ and increased faster, leading to the faster drop of ΔT_{P1}. Because of a small melting peak in 12-15 ℃ for PCMNE in the 39th cycle, its ΔT_{P1} fell in between ΔT_{P1} of PCMNE (3rd cycle) and water. It should be noted that T_{in} was obviously higher than the temperature of bottom layer in tank (T_4), because the RTD was attached at the surface of copper pipe that caused a measurement error at the low temperature. As the measurement of T_{in} was more accurate at a higher fluid temperature (>12 ℃), the LHTES performance evaluation of this study has been calculated based on the four RTDs in the storage tank. On the other hand, the maximum $q_{d,avg}$ can be estimated to over 300 W at the beginning of discharging because of the maximum temperature difference (>20 ℃) between T_{in} and T_{out}. After the period of 30 min for cooled PCMNE filling in ceiling panels, $q_{d,avg}$ started to decrease from around 250 W to

below 200 W for the end of discharging.

4. Conclusions

In the present study, the application of a novel phase change material nano-emulsion for cooling energy storage has been successfully demonstrated in a self-designed, pilot-scale latent heat thermal storage unit with regeneration function. The nano-emulsion with a total volume of 60 L (~5 L tap water dilution) showed a high dynamic stability through repeated charging (freezing) and discharging (melting) cycles in the pilot unit under operation for more than two months, during which the cooling performance remained almost unchanged. The nano-emulsion could be easily regenerated to retain nearly the original properties. The robustness and regeneration capability ensure a long service life as the cooling fluid for room air-conditioning application. During the operation, the nano-emulsion could achieve rapid charging of cooling energy from the chiller at an average charging rate of 770-800 W and near 1.4 kW during the phase transition process. Compared with water, it showed a much higher thermal storage capacity and the high efficiency of cooling energy release, which help compensate for the higher material cost in commercial application. However, more research effort is needed to overcome the high degree of supercooling so as to increase the energy efficiency.

Acknowledgments

This work was supported financially by the Environment and Conservation Fund (ECF 588 Project 53/2018), the Research Grant Council of the Hong Kong SAR Government through General Research Fund (PolyU 152707/16E), and by the Hong Kong Polytechnic University. The authors are grateful to Jing Li's support to the design and construction of the pilot unit.

References

[1] Nazir H, Batool M, Bolivar Osorio FJ, Isaza-Ruiz M, Xu X, Vignarooban K, et al. Recent developments in phase change materials for energy storage applications: A review. International Journal of Heat and Mass Transfer. 2019;129:491-523.

[2] Souayfane F, Fardoun F, Biwole P-H. Phase change materials (PCM) for cooling

applications in buildings: A review. Energy and Buildings. 2016;129:396-431.

[3] Sciacovelli A, Gagliardi F, Verda V. Maximization of performance of a PCM latent heat storage system with innovative fins. Applied Energy. 2015;137:707-15.

[4] Mahdi JM, Nsofor EC. Solidification enhancement of PCM in a triplex-tube thermal energy storage system with nanoparticles and fins. Applied Energy. 2018;211:975-86.

[5] Parsazadeh M, Duan X. Numerical study on the effects of fins and nanoparticles in a shell and tube phase change thermal energy storage unit. Applied Energy. 2018;216:142-56.

[6] Tao YB, Lin CH, He YL. Preparation and thermal properties characterization of carbonate salt/carbon nanomaterial composite phase change material. Energy Conversion and Management. 2015;97:103-10.

[7] Fan L-W, Fang X, Wang X, Zeng Y, Xiao Y-Q, Yu Z-T, et al. Effects of various carbon nanofillers on the thermal conductivity and energy storage properties of paraffin-based nanocomposite phase change materials. Applied Energy. 2013;110:163-72.

[8] Ling Z, Chen J, Xu T, Fang X, Gao X, Zhang Z. Thermal conductivity of an organic phase change material/expanded graphite composite across the phase change temperature range and a novel thermal conductivity model. Energy Conversion and Management. 2015;102:202-8.

[9] Xu T, Chen Q, Huang G, Zhang Z, Gao X, Lu S. Preparation and thermal energy storage properties of d-Mannitol/expanded graphite composite phase change material. Solar Energy Materials and Solar Cells. 2016;155:141-6.

[10] Wang F, Zhang C, Liu J, Fang X, Zhang Z. Highly stable graphite nanoparticle-dispersed phase change emulsions with little supercooling and high thermal conductivity for cold energy storage. Applied Energy. 2017;188:97-106.

[11] Cui W, Yuan Y, Sun L, Cao X, Yang X. Experimental studies on the supercooling and melting/freezing characteristics of nano-copper/sodium acetate trihydrate composite phase change materials. Renewable Energy. 2016;99:1029-37.

[12] Tian H, Du L, Wei X, Deng S, Wang W, Ding J. Enhanced thermal conductivity of ternary carbonate salt phase change material with Mg particles for solar thermal energy storage. Applied Energy. 2017;204:525-30.

[13] Şahan N, Fois M, Paksoy H. Improving thermal conductivity phase change materials—A study of paraffin nanomagnetite composites. Solar Energy Materials and Solar Cells. 2015;137:61-7.

[14] Xiao X, Zhang P, Li M. Preparation and thermal characterization of paraffin/metal foam composite phase change material. Applied Energy. 2013;112:1357-66.

[15] Huang X, Lin Y, Alva G, Fang G. Thermal properties and thermal conductivity enhancement of composite phase change materials using myristyl alcohol/metal foam for solar thermal storage. Solar Energy Materials and Solar Cells. 2017;170:68-76.

[16] Fang Y, Xu H, Miao Y, Bai Z, Niu J, Deng S. Experimental study of storage capacity and discharging rate of latent heat thermal energy storage units. Applied Energy. 2020;275:115325.

[17] Wang F, Lin W, Ling Z, Fang X. A comprehensive review on phase change material emulsions: Fabrication, characteristics, and heat transfer performance. Solar Energy Materials and Solar Cells. 2019;191:218-34.

[18] Chen J, Zhang P. Preparation and characterization of nano-sized phase change emulsions as thermal energy storage and transport media. Applied Energy. 2017;190:868-79.

[19] Liu L, Niu J, Wu J-Y. Formulation of highly stable PCM nano-emulsions with reduced supercooling for thermal energy storage using surfactant mixtures. Solar Energy Materials and Solar Cells. 2021;223:110983.

[20] Ma F, Chen J, Zhang P. Experimental study of the hydraulic and thermal performances of nano-sized phase change emulsion in horizontal mini-tubes. Energy. 2018;149:944-53.

[21] Morimoto T, Kumano H. Flow and heat transfer characteristics of phase change emulsions in a circular tube: Part 1. Laminar flow. International Journal of Heat and Mass Transfer. 2018;117:887-95.

[22] Morimoto T, Kumano H. Flow and heat transfer characteristics of phase change emulsions in a circular tube: Part 2. Turbulent flow. International Journal of Heat and Mass Transfer. 2018;117:903-11.

[23] Morimoto T, Suzuki K, Kumano H. Heat transfer characteristics of phase change emulsions with solidification of phase change material particles in a circular tube. International

Journal of Refrigeration. 2020;114:1-9.

[24] Morimoto T, Sugiyama M, Kumano H. Experimental study of heat transfer characteristics of phase change material emulsions in a horizontal circular tube. Applied Thermal Engineering. 2021;188:116634.

[25] Cao J, He Y, Feng J, Lin S, Ling Z, Zhang Z, et al. Mini-channel cold plate with nano phase change material emulsion for Li-ion battery under high-rate discharge. Applied Energy. 2020;279:115808.

[26] Feng J, Huang J, Ling Z, Fang X, Zhang Z. Performance enhancement of a photovoltaic module using phase change material nanoemulsion as a novel cooling fluid. Solar Energy Materials and Solar Cells. 2021;225:111060.

[27] Liu L, Li J, Niu J, Wu J-Y. Evaluation of the energy storage performance of PCM nano-emulsion in a small tubular heat exchanger. Case Studies in Thermal Engineering. 2021;26:101156.

[28] Delgado M, Lázaro A, Mazo J, Peñalosa C, Marín JM, Zalba B. Experimental analysis of a coiled stirred tank containing a low cost PCM emulsion as a thermal energy storage system. Energy. 2017;138:590-601.

[29] Delgado M, Lázaro A, Mazo J, Peñalosa C, Dolado P, Zalba B. Experimental analysis of a low cost phase change material emulsion for its use as thermal storage system. Energy Conversion and Management. 2015;106:201-12.

[30] Biedenbach M, Poetzsch L, Gschwander S. Characterization of an n-octadecane PCS in a 0.5 m^3 storage tank test facility. International Journal of Refrigeration. 2019;104:76-83.

[31] Fernandez P, André V, Rieger J, Kühnle A. Nano-emulsion formation by emulsion phase inversion. Colloids and Surfaces A: Physicochemical and Engineering Aspects. 2004;251:53-8.

[32] Zhang S, Niu J. Two performance indices of TES apparatus: Comparison of MPCM slurry vs. stratified water storage tank. Energy and Buildings. 2016;127:512-20.

[33] Ning B, Chen Y, Liu H, Zhang S. Cooling capacity improvement for a radiant ceiling panel with uniform surface temperature distribution. Building and Environment. 2016;102:64-

72.

[34] Zhang P, Ma ZW, Bai ZY, Ye J. Rheological and energy transport characteristics of a phase change material slurry. Energy. 2016;106:63-72.

[35] Zhang X, Niu J, Wu J-y. Evaluation and manipulation of the key emulsification factors toward highly stable PCM-water nano-emulsions for thermal energy storage. Solar Energy Materials and Solar Cells. 2021;219:110820.

[36] Zhang X, Niu J, Wu J-Y. Development and characterization of novel and stable silicon nanoparticles-embedded PCM-in-water emulsions for thermal energy storage. Applied Energy. 2019;238:1407-16.

[37] Morimoto T, Kawana Y, Saegusa K, Kumano H. Supercooling characteristics of phase change material particles within phase change emulsions. International Journal of Refrigeration. 2019;99:1-7.

[38] Xu H, Miao Y, Wang N, Qu Z, Wang X. Experimental investigations of heat transfer characteristics of MPCM during charging. Applied Thermal Engineering. 2018;144:721-5.

[39] Wang F, Fang X, Zhang Z. Preparation of phase change material emulsions with good stability and little supercooling by using a mixed polymeric emulsifier for thermal energy storage. Solar Energy Materials and Solar Cells. 2018;176:381-90.

Supplementary data

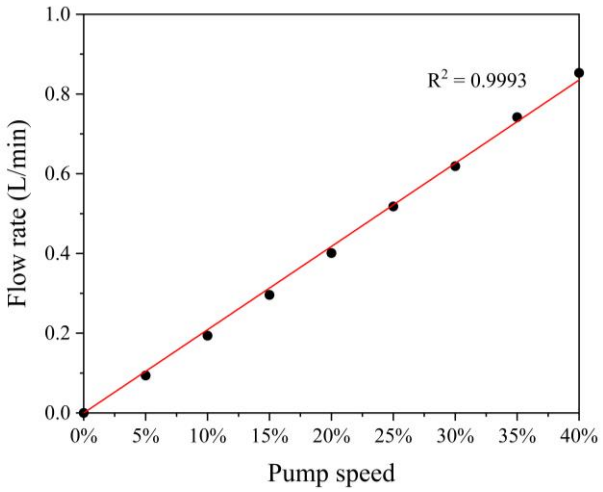

Fig. S1 Flow rate calibration curve of a diaphragm metering pump as a function of pump speed.

Table S1 Thermal properties of PCMNE with 45 charging-discharging cycles in the pilot unit.

PCMNE	ΔH_m (J/g)	ΔH_f (J/g)	Onset T_m (℃)	Onset T_f (℃)	ΔT (℃)
5^{th} cycle	-35.2	36.6	12.6	9.6	3.0
10^{th} cycle	-34.8	35.8	17.1	7.1	10.0
35^{th} cycle	-34.6	36.8	16.8	5.5	11.3
40^{th} cycle	-34.1	35.1	16.7	5.8	10.9
45^{th} cycle	-34.3	37.5	16.9	5.3	11.6
Regeneration	-34.0	38.1	12.8	10.0	2.8

Fig. S2 Photographs of PCMNEs showing a uniform state after 45 cycles which could remain stable for extra 8 months at room temperature. The regenerated PCMNE presented a slight appearance variation in comparison to the original one, due to the existence of Fe ions mainly coming from RTDs package.